Fiber IFU unit for the second generation VLT spectrograph KMOS

Daigo Tomono[a], Harald Weisz[b], and Reiner Hofmann[a]

[a]MPE, Giessenbachstraße 1, 85748 Garching, Germany
[b]Ingenieurbüro für den Maschinenbau, Menzinger Straße 1, 80638 München, Germany

ABSTRACT

KMOS is a cryogenic multi-object near-infrared spectrograph for the VLT. It will be equipped with about 20 deployable integral field units (IFUs) which can be positioned anywhere in the 7.2 arcmin diameter field of the VLT Nasmyth focus by a cryogenic robot. We describe IFUs using micro lens arrays and optical fibers to arrange the two-dimensional fields from the IFUs on the spectrograph entrance slit. Each micro-lens array is mounted in a spider arm which also houses the pre-optics with a cold stop. The spider arms are positioned by a cryogenic robot which is built around the image plane. For the IFUs, two solutions are considered: monolithic micro-lens arrays with fibers attached to the back where the entrance pupil is imaged, and tapered fibers with integrated lenses which are bundled together to form a lens array. The flexibility of optical fibers relaxes boundary conditions for integration of the instrument components. On the other hand, FRD and geometric characteristics of optical fibers leads to higher $A\Omega$ accepted by the spectrograph. Conceptual design of the instrument is presented as well as advantages and disadvantages of the fiber IFUs.

Keywords: IFU, optical fiber, robot, cryogenic, NIR

1. INTRODUCTION

Recently, needs for spectral samples of high red shift galaxies are increasing. For more understanding of the galaxy evolution history, we need to measure the star formation history at a high red shift. It is known from observations in the visible wavelength (e.g. Reference 1) that the star formation rate is higher at higher red shift within $z \lesssim 1$. Star formation rates at $z \gtrsim 3$ are measured, using luminosity of the rest UV continuum, to be lower than that of the $z \sim 1$ galaxies. It seems that there is a peak of the star formation rate at $z \sim 2$.[2] Nevertheless, the UV continua are strongly attenuated by dust inside the observed galaxies. With a certain assumption on absorption correction, star formation rate increases beyond $z \sim 4$.[3] Therefore, more reliable measurements of star formation rate at $z \gtrsim 2$ are required. In this red shift range, the Hα line, which is a good index of star formation, drops in the K-band. Also, intensity of the Hβ line, observable in the H-band, can be used to determine dust absorption when compared with the Hα intensity. Moreover, emission lines such as [N II]6584 Å and [O II]5007 Å observable in the H- and K-bands can be used to estimate metallicity and electron density. Systematic samples of near-infrared (NIR) spectra will play an important roll in understanding the history of the universe. However, it takes hours to obtain spectra of the high-z galaxies with a reasonable signal-to-noise (SN) ratio as shown in Figure 1. Therefore, systematic observations, have been rather limited to a small number (e.g. Reference 4). While new survey projects (e.g. Reference 5) are planned and a huge number of high-z objects is expected to be discovered, it is necessary to build a spectrometer which can observe a number of targets at the same time to overcome this limitation. In this paper, we describe a design of a NIR multi-object spectrometer using optical fibers.

This study is a collaboration of UK and German institutes for the VLT second generation instrument. Reference 6 describes the complete instrument with two IFU options: image slicer[7] and fiber/micro-lens (this paper).

2. INSTRUMENT CHARACTERISTICS

The instrument aims to take NIR spectra of diffuse targets with the maximum multiplex gain. As shown in the previous section, it is important to cover the K-band. This section shows required characteristics of such an instrument.

Figure 2 shows an estimation of the number of sources observable in the field of view (FOV) on a 8-m class telescope. From 10 to 50 of $z>2$ galaxies are expected to be observable with limiting magnitude of 20.5 – 21 in the K-band. Therefore, roughly 20 targets must be observed at the same time to maximize the multiplex gain.

Further author information: (Send correspondence to D.T.)
D.T.: E-mail: tomono@mpe.mpg.de, Telephone: +49 (0)89 30000 3509

Instrument Design and Performance for Optical/Infrared Ground-based Telescopes,
Masanori Iye, Alan F. M. Moorwood, Editors, Proceedings of SPIE Vol. 4841 (2003)

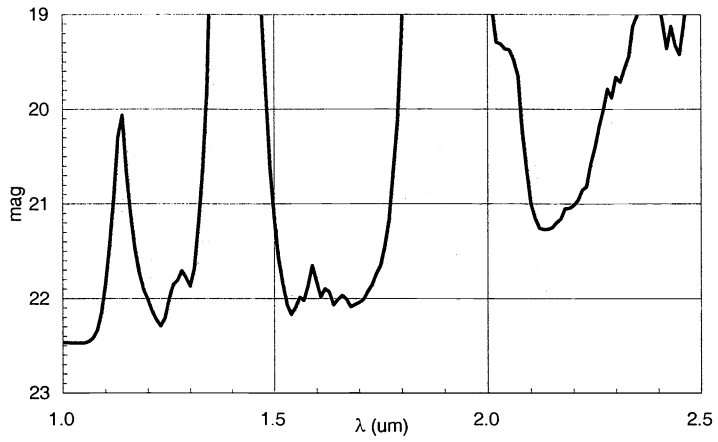

Figure 1. Estimated point source sensitivity for 6 hours on-source integration at 5σ with spectral elements rebinned to have spectral resolving power of 1000 after software suppression of OH sky lines. FOV of a spatial element is assumed to be $0.2''\phi$ with a point source spreading over 4 spatial elements.

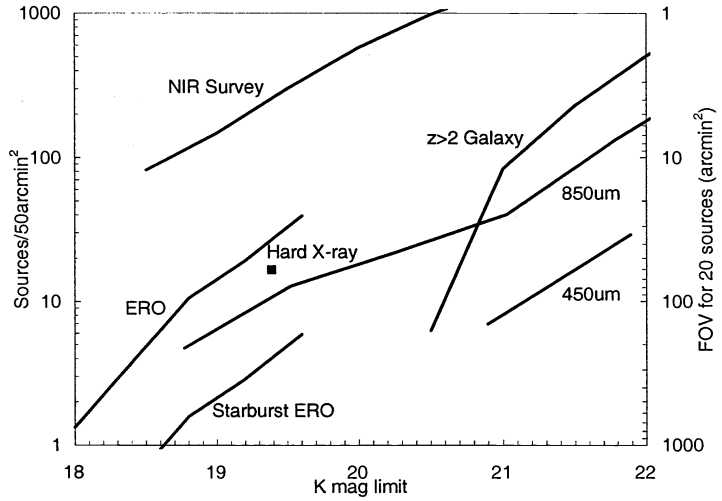

Figure 2. Cumulative source number densities of high-z sources. References: NIR Survey[8], z>2 Galaxy[89], Hard X-ray[10], 450 and 800 μm[1112], ERO[13], and Starburst ERO[1314].

Table 1. Baseline parameters of KMOS

Wavelength coverage	J, H, and K-bands	
Spectral resolution	4000	
IFU patrol field	$7.2'\phi$	
Number of IFUs	$\sim$20	
Spatial resolution	$0.2''$ (seeing)	$0.1''$ (MCAO)
Spatial elements/IFU	$\sim$100	
IFU FOV	$\sim 2'' \times 2''$	$\sim 1'' \times 1''$
FPA	6 of 2048$\times$2048 pixels	

For higher sensitivity, it is necessary to obtain sky background from the sky adjacent to the target. It is also important to spatially resolve the target so that we can be sure that the target is inside the FOV of the IFU and its luminosity is measured correctly. For these two reasons, integral field units (IFUs), which re-arrange spatial elements onto the entrance slit of the spectrograph, have to be integrated. When the positions of the IFUs are checked, the grating of the spectrograph is replaced with a mirror for higher sensitivity. The FOV of each IFU must be large enough in comparison with the typical target size for sky subtraction and in comparison with the proposed positional accuracy of the new surveys. This eliminates the need for an integrated wide-field imager, which adds complexity to the instrument, to check the target position. Moreover, for low-z objects, the IFUs will reveal dynamical motion inside the target. Besides IFUs for target observation, a couple of imaging IFUs centered on stars are assigned to monitor the telescope pointing and of IFU movement. We also have to consider feasibility of re-arranging the IFUs during integration to observe objects with different brightness with appropriate integration times.

Spectral resolution $\lambda/\delta\lambda$ must be $\gtrsim$ 4000 to avoid OH sky lines.[15] This also enables us to assess dynamical structure of spatially resolved targets. About 1000 spectral elements have to be sampled to cover each of the three band J, H, or K with one exposure. This requires us to use focal plane arrays (FPAs) of 2000$\times$2000 pixels. With an FPA of 2000$\times$2000 pixels, up to 1000 spatial elements can be sampled. Moreover, for high-z targets with unknown red shift and for low-z targets with a number of detectable emission lines, simultaneous exposure in the three bands enhances the multiplex gain. We have to note that SN ratio will be higher in shorter wavelength than in longer wavelength where we suffer from thermal background radiation.

Seeing limited observations are primary considered in this paper. Diffraction limited spatial resolution delivered by the multi conjugate adaptive optics (MCAO) is also considered as an option. Table 1 shows basic parameters required to realize such an instrument. IFUs need to be deployed anywhere on the telescope FOV. In the field, 10–50 of targets are expected. To observe 20 of them with required spatial resolution and required IFU FOV, 2000 spatial elements are to be sampled at a time. This requires two FPAs for each band. Therefore, six FPAs in total are required for the three bands.

3. IFU DESIGN

We assess the feasibility of a multi-object spectrometer using optical fibers to arrange the two-dimensional field onto the spectrograph. See Reference 7 for consideration about IFUs using image slicers. Advantages and disadvantages of the fibers are described in the following sections.

Optical fibers have a big advantage in freedom of component arrangements over the mechanical light guides. With the flexibility, spherical image surface as shown in Figure 4 can be adopted and the spectrograph can be located rather freely. Observing in the K-band, IFUs have to be cooled down to $\sim$ 100 K to reduce thermal emission from the instrument below the background emission. Silica fibers remain flexible at cryogenic temperatures and only negligible excess focal ratio degradation occurs when fibers are cooled.[16] Each IFU is mounted at the tip of spiders, which is held by magnets on a mounting plate or sphere. The spiders are moved by the cryogenic robot and assigned to each target. [17]

On the other hand, there are a number of disadvantages. First, fibers have focal radio degradation (FRD). [18] With other effects described in the following sections, the spectrograph has to accept $\sim$ 7 times bigger AΩ than that of the incoming light to avoid lower efficiency. Second, silica fibers have absorption bands due to OH contamination around 1.4 μm and beyond $\sim$ 2.2 μm. Recently, the telecommunication industry is beginning to use the 1.4 μm band (E-band: 1.36–1.45 μm) for Course Wave Division Multiplexing (CWDM) applications, which requires 'low-water peak' fibers. This is a favorable situation for us because it might make it easier to obtain low OH contamination fibers, which might also have higher transmittance in the

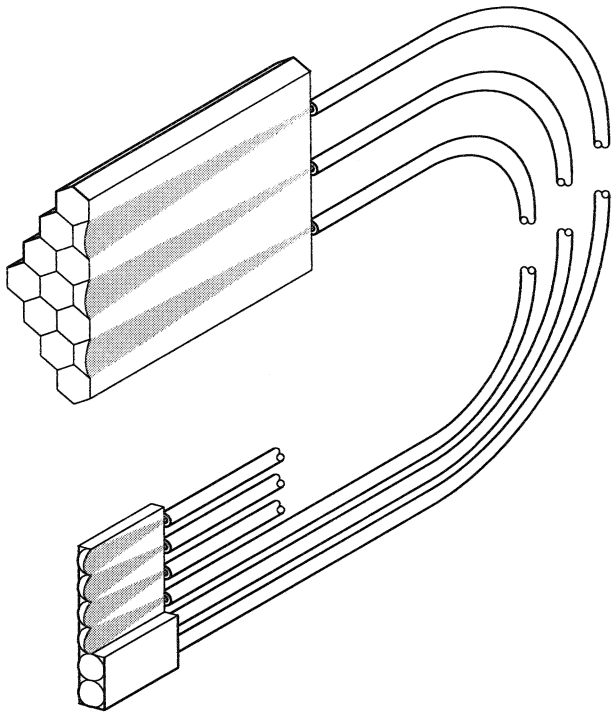

Figure 3. Optical train from an IFU to a slit micro lens array. This illustrates an example using micro lens arrays, which is optically the same when tapered fibers are used. Shade shows the cross sections of rays going into/emerging from the fibers. Hexagonal micro lens array is located on the image plane and images entrance pupil onto each fiber. Light is transfered through the fibers into the slit micro lens. The slit micro lens array images the scrambled image plane onto pseudo slit as shown in Figure 7.

K-band. Still, length of the fibers is limited to about 1 m. Third, the beam profile emerging from the fibers might change with physical movements of the fibers and change of temperature. This might change the instrumental spectral profile. These problems have to be quantified through experiments.

4. OPTICAL TRAIN

In this section, we discuss in more detail the optical train leading the light from the telescope into the entrance slit of the spectrograph. Figure 3 shows the optical components between the IFU and the entrance slit of the spectrograph. Example designs of the field lens and the pre-optics are shown in Figures 4 and 5.

4.1. Cold stop and field lens

To observe in the K-band, a cold stop is required for each IFU to reduce thermal emission from the telescope structure. As optical fibers scramble the light, the stop has to be in the up stream of the fibers. Therefore, a pre-optics integrated in each IFU is needed to image the telescope entrance pupil onto the cold stop.

With the wide patrol FOV of the IFUs, we have to take into account the change of the beam direction. In case IFUs are mounted and moved on a flat surface, 4 % of the beams going through the cold stop come from outside of the telescope entrance pupil at the edge of the $7.2'\phi$ FOV. The VLT has a field curvature radius of 2.0 m with the center of curvature on the telescope side. The field curvature radius is still too small in comparison with the distance to the telescope entrance pupil (the secondary mirror) of 16.7 m. Therefore, even if the IFUs are mounted on the focal sphere of the telescope, thermal background from outside of the entrance pupil is introduced. Therefore, a field lens have to be placed between the telescope and the IFUs, to at least direct incoming beams perpendicular to the sphere where IFUs are mounted on. Figure 4 shows an example design of the field lens. The first lens also serves as the entrance window of the cryostat.

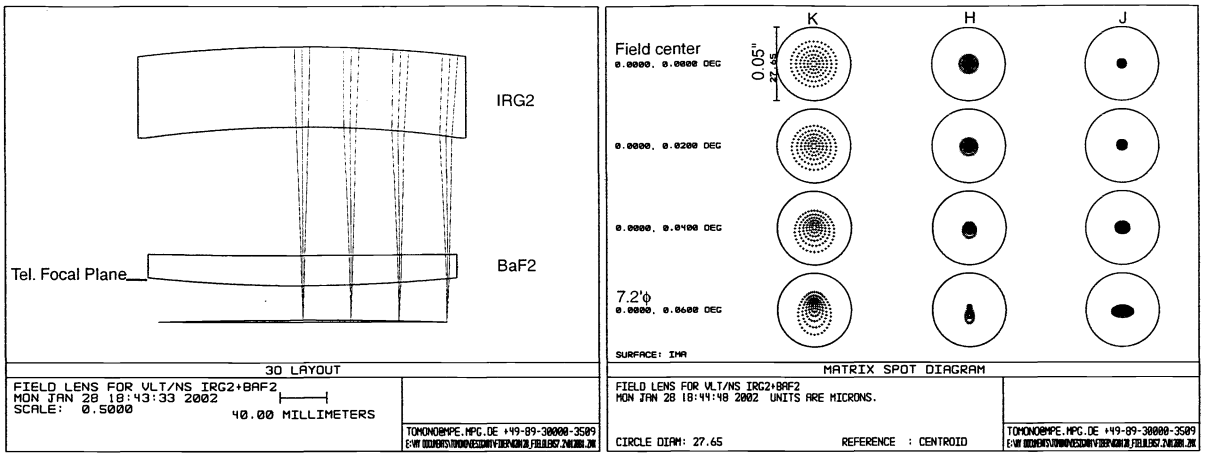

Figure 4. An example design of field lens which images the field onto a sphere with 4.3 m radius and makes the beam perpendicular to it. The left panel shows the lens layout. The IRG2 lens has a diameter of 280 mm while the BaF_2 lens has a diameter of 265mm. First surface of the IRG2 lens is 20 cm into the telescope from the telescope focal plane. The right panel shows that the geometric spot diameter is less than 0.05″. Entrance pupil image on the IFUs mounted on the field sphere moves less than 0.1 % of its diameter on the 7.2′ϕ FOV.

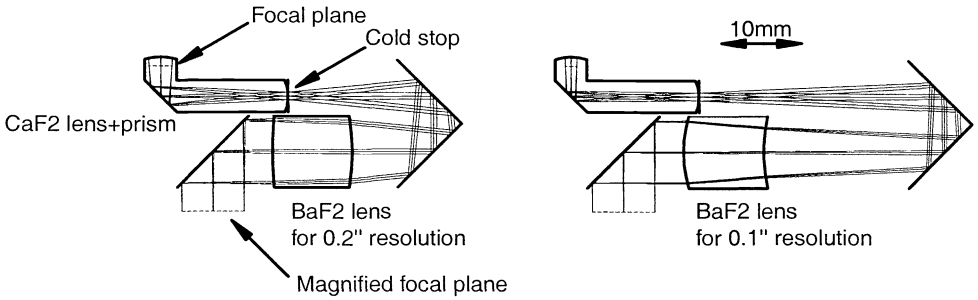

Figure 5. Pre-optics to be integrated into an IFU on the spherical image surface. It images the entrance pupil onto the cold stop, adjusts the plate scale, and makes a telecentric beam. The panels show two configurations of the pre-optics with plate scales on the IFU of 0.2″/0.3mm (left) and 0.1″/0.3mm (right). Every surfaces are spherical. Plate scales can be changed with exchanging the BaF_2 lens and the corner mirror. The cold stop is integrated on the surface of the CaF_2 lens. The image quality in J-, H-, and K-bands is about 10 μm rms radius.

We are also considering an option to integrate a re-imaging K-mirror. A three-mirror off-axis re-imaging optics with two flat mirrors can be laid out so that it acts as an image de-rotator. If it can be designed to provide a telecentric beam with a flat focal plane, it makes it even easier to design the cryogenic robot to arrange the IFUs on the focal plane than to arrange them on the focal sphere.

4.2. Pre-optics and micro lens arrays

With the circular cross sections of the fibers and a certain thickness of cladding layer, field filling factor of the cores of the fibers in a bundle is quite low. Therefore, a micro lens array or a tapered fiber on the image plane has to be integrated to image the entrance pupil onto the fiber core. A hexagonal configuration is considered to obtain maximum filling factor and the lowest AΩ output,

The 0.2″ spatial resolution corresponds to a linear size of 0.12 mm on the image plane. With the practical size of a micro lens being $\sim$ 0.3 mm, the image have to be magnified before getting into the micro lens array or the tapered fiber. Therefore, the pre-optics is designed to have proper magnification. It also images the entrance pupil onto the cold stop as stated in the previous section. Figure 5 shows an example design.

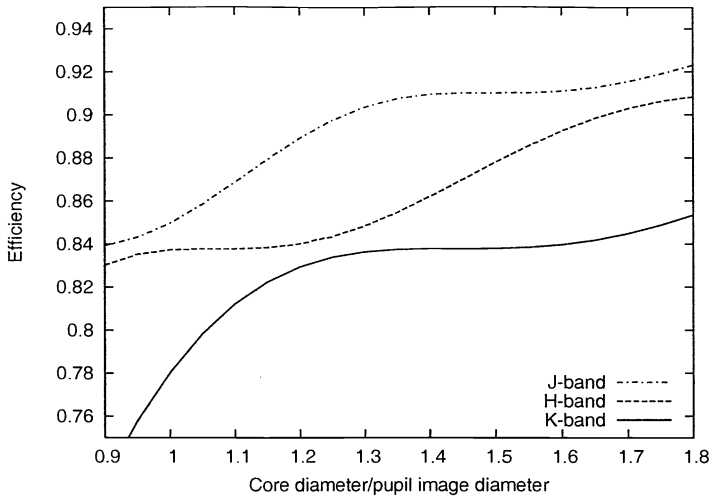

Figure 6. Diffraction coupling efficiency between the micro lens and the fiber. Diffraction pattern of the pupil imaged by the micro lens is integrated on the fiber core. Spatial resolution of $0.2''$ and fiber core diameter of 50 μm are assumed.

In the K-band, diffraction becomes important on the fiber core. When the image of the entrance pupil by the micro lens is the same size as the fiber core of 50 μm, coupling efficiency between the micro lens and the fiber is 78 % in K-band. As shown in Figure 6, when the image diameter is $\sim$ 1.4 times smaller, coupling efficiency is about 84 %. Because the image is scrambled in the fiber, AΩ of the emergent light becomes $\sim$ 2 times bigger than that of the incident light.

4.3. Pseudo slit

On the entrance slit of the spectrograph, the exits of the fibers are lined up. Because cross talk between the spatial elements can not be perfectly avoided, the fibers have to be aligned on a straight line to avoid wavelength shift between the spatial elements. Indeed, the influence of cross talk can be minimized when the neighboring fibers on the spectrograph entrance slit are neighboring spatial elements on the sky.[19]

With the cladding thickness, length of the slit becomes bigger than the length needed just for the cores of the fibers. Therefore, the spectrometer must accept bigger AΩ than that for the light emitted from the fibers. The situation can be relaxed when we integrate a one-dimensional micro lens array on the slit.

From geometrical calculations, effective AΩ, which is defined as product of the area of the pseudo slit and the solid angle of the light, becomes $4/\pi \times r_{clad}/r_{core} \sim 2.55$ times bigger for a fiber with core radius of r_{core} and cladding radius of r_{clad}*. With a micro lens, a pseudo slit image with width of w_{slit} can be imaged. In the case, change of effective AΩ is $4/\pi \times (1+2 \times r_{core}/w_{slit}) \sim 1.70$*. Figure 7 shows an example design of slit micro lens compared with bare fibers. Length of the pseudo slit is longer with the slit micro lens than that for the bare fibers. But with the slower light, effective AΩ is smaller.

5. CONCLUSION

We have described a NIR multi-object spectrometer which employs IFUs that are connected to the entrance slit of the spectrograph with optical fibers. This solution has an advantage of the flexibility in arrangement of components because the optical fibers can be bent freely even at the cryogenic temperature. This enables us to adopt spherical image surface with concentric beams forming the image, which has higher image quality than making a telecentric image plane. Also, the spectrograph can be located more freely than using mechanical light guides. On the other hand, the spectrograph have to accept higher AΩ. This is due to FRD of the fibers as well as its geometric characteristics: small core diameter comparable to diffraction and

*A fiber with $r_{core} = 25\mu$m, $r_{clad} = 50\mu$m and pseudo slit image with width of $w_{slit} = 150\mu$m image are assumed.

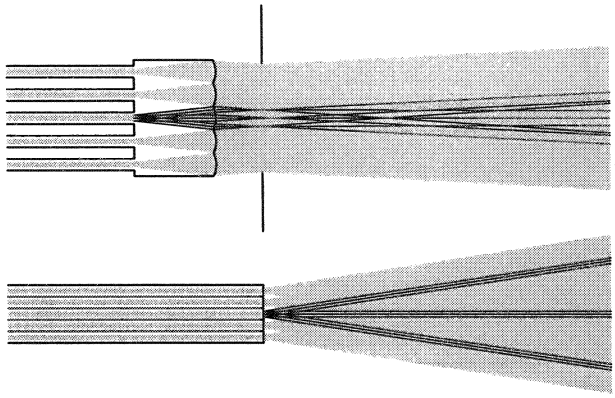

Figure 7. An example ray trace for slit micro lens compared with bare fibers. Five spatial elements are shown to illustrate the effect of the slit micro lens. Thin lines represent rays from the middle fiber with shade showing the envelope of the rays for all of the fibers. Top plate shows the fibers with a pseudo slit imaged by the micro lens array Bottom plate shows the five bare fibers forming a slit. The pseudo slit imaged by the micro lens array is bigger than the bundle of bare fibers. Though, with light cone angle smaller than that for the bare fibers, effective AΩ is smaller than that for the bare fibers.

cladding thickness comparable to core diameter. We have to clarify these characteristics to quantify the needed AΩ. Moreover a spectrograph that accepts appropriate AΩ has to be designed.

Currently, we are testing the proto-type of the cryogenic robot, measuring a number of fibers, and investigating the feasibility of producing micro lens arrays and tapered fibers.

REFERENCES

1. S. J. Lilly, O. Le Fevre, F. Hammer, and D. Crampton, "The Canada-France Redshift Survey: The Luminosity Density and Star Formation History of the Universe to Z approximately 1," ApJ **460**, pp. L1–L4, Mar. 1996.
2. P. Madau, H. C. Ferguson, M. E. Dickinson, M. Giavalisco, C. C. Steidel, and A. Fruchter, "High-redshift galaxies in the Hubble Deep Field: colour selection and star formation history to z∼4," MNRAS **283**, pp. 1388–1404, Dec. 1996.
3. C. C. Steidel, K. L. Adelberger, M. Giavalisco, M. Dickinson, and M. Pettini, "Lyman-Break Galaxies at $z \gtrsim 4$ and the Evolution of the Ultraviolet Luminosity Density at High Redshift," ApJ **519**, pp. 1–17, July 1999.
4. A. F. M. Moorwood, P. P. van der Werf, J. G. Cuby, and E. Oliva, "Hα emitting galaxies and the cosmic star formation rate at $z \simeq 2.2$," A&A **362**, pp. 9–18, Oct. 2000.
5. J. P. Emerson, "VISTA - Project Status of the Visible and Infrared Survey Telescope for Astronomy.," in *ASP Conf. Ser. 232: The New Era of Wide Field Astronomy*, pp. 339–346, 2001.
6. R. M. Sharples, R. Bender, R. Hofmann, R. Genzel, and I. R. J., "KMOS: an infrared multi-integral field spectrograph for the VLT.".
7. S. K. Ramsay-Howat et al., "Multiple integral field spectroscopy using image slicers." in these proceedings.
8. M. A. Bershady, J. D. Lowenthal, and D. C. Koo, "Near-Infrared Galaxy Counts to J and K $\sim$ 24 as a Function of Image Size," ApJ **505**, pp. 50–73, Sept. 1998.
9. J. G. Cohen, D. W. Hogg, R. Blandford, L. L. Cowie, E. Hu, A. Songaila, P. Shopbell, and K. Richberg, "Caltech Faint Galaxy Redshift Survey. X. A Redshift Survey in the Region of the Hubble Deep Field North," ApJ **538**, pp. 29–52, July 2000.
10. R. Giacconi, P. Rosati, P. Tozzi, M. Nonino, G. Hasinger, C. Norman, J. Bergeron, S. Borgani, R. Gilli, R. Gilmozzi, and W. Zheng, "First Results from the X-Ray and Optical Survey of the Chandra Deep Field South," ApJ **551**, pp. 624–634, Apr. 2001.
11. A. W. Blain, J.-P. Kneib, R. J. Ivison, and I. Smail, "Deep Counts of Submillimeter Galaxies," ApJ **512**, pp. L87–L90, Feb. 1999.
12. R. J. Ivison, I. Smail, A. J. Barger, J.-P. Kneib, A. W. Blain, F. N. Owen, T. H. Kerr, and L. L. Cowie, "The diversity of SCUBA-selected galaxies," MNRAS **315**, pp. 209–222, June 2000.

13. E. Daddi, A. Cimatti, and A. Renzini, "EROs and the formation epoch of field ellipticals," A&A **362**, pp. L45–L48, Oct. 2000.
14. G. Moriondo, A. Cimatti, and E. Daddi, "The morphology of extremely red objects," A&A **364**, pp. 26–42, Dec. 2000.
15. S. Mengel, F. Eisenhauer, M. Tecza, N. A. Thatte, C. Roehrle, K. Bickert, and J. Schreiber, "New era of spectroscopy: SINFONI NIR integral field spectroscopy at the diffraction limit of an 8-m telescope," in *Proc. SPIE Vol. 4005, p. 301-309, Discoveries and Research Prospects from 8- to 10-Meter-Class Telescopes, Jacqueline Bergeron; Ed.*, **4005**, pp. 301–309, June 2000.
16. D. Lee, R. Haynes, and D. J. Skeen, "Properties of optical fibres at cryogenic temperatures," MNRAS **326**, pp. 774–780, Sept. 2001.
17. R. Genzel, R. Hofmann, D. Tomono, N. A. Thatte, F. Eisenhauer, M. Tecza, and R. Bender, "CROMOS: A cryogenic near-infrared, multi-object spectrometer for the VLT." to be published in the Proc. of the ESO Workshop Scientific Drivers for ESO Future VLT/VLTI Instrumentation held in Garching, Germany, 11-15 June 2001, astro-ph/0108318.
18. E. Carrasco and I. R. Parry, "A method for determining the focal ratio degradation of optical fibres for astronomy," MNRAS **271**, pp. 1–12, Nov. 1994.
19. J. Allington-Smith and R. Content, "Sampling and Background Subtraction in Fiber-Lenslet Integral Field Spectrographs," PASP **110**, pp. 1216–1234, Oct. 1998.